Precise Timescale for Research Advancements

Jahnvi Verma†, August Connors, Nischal Bhattarai, Charles Rasor and Thejesh Bandi‡
Department of Physics and Astronomy, Tuscaloosa, USA
Email: †jverma@crimson.ua.edu; ‡tbandi@ua.edu

***Abstract*—We report the development and testing of the three different Kalman filter based algorithms for a new timescale at the University of Alabama (UA), with a vision for utilizing this as a unique test-bed for the *timescale* and *time transfer* research advancements for the future precise timekeeping. The Outlier Robust Kalman Filter (ORKF) has been implemented and tested in a timescale for the first time. A successful demonstration and characterization of different Kalman filters and weighting algorithms using three cesium clocks and one active hydrogen maser (AHM) is reported. Our timescale will have additional two AHMs in future making it a robust platform for algorithms testing geared towards the neural network methods.**

***Index Terms*—Kalman filter; Time-frequency analysis; Frequency and time transfer; Frequency synchronization; Timescale; Clock Ensemble; Kalman Filtering; neural networks**

I. Introduction

Precision timekeeping is the basis for maintaining the International Atomic Time (TAI) – as a weighted average of the contributions by about 480 clocks from various metrology labs around the world. The conventional method of timekeeping needs a relook in terms of the algorithms and diligent utilization of big data for improving the accuracies and reliability [1]. Redefinition of the time may need evaluating new algorithms, prior to the actual implementation in TAI [2], [3]. We are developing a timescale focused on the advancements for precision timekeeping that is flexible for research and testing with various different algorithms and to include any new type of clock (microwave or optical) in future for feasibility testing purposes. This would help for prior determination of its impact on an actual timekeeping system in any national metrology lab.

This work details our efforts on implemented three different Kalman filter designs with four different weighting algorithms in our timescale. The paper presents the measured results and comparison of these various methods with a future outlook.

II. Timescale Realization

A. Timescale system

The timescale utilizes three Cesium Clocks and one Active Hydrogen Maser (AHM). All the clocks run at the standard frequency of 5 MHz. A multi-channel measurement system is used to collect the phase signals from all the clocks, by comparing the inputs with its internal oscillator (TSC 2049 quartz oscillator), and streamlining the outputs as phase differences at every second measurement interval. To eliminate the internal oscillator component, these phase differences corresponding to the four clocks are then compared against each other, at every time-step. Therefore, we have six phase measurements every second. The stability results in the fig. 1 shows the

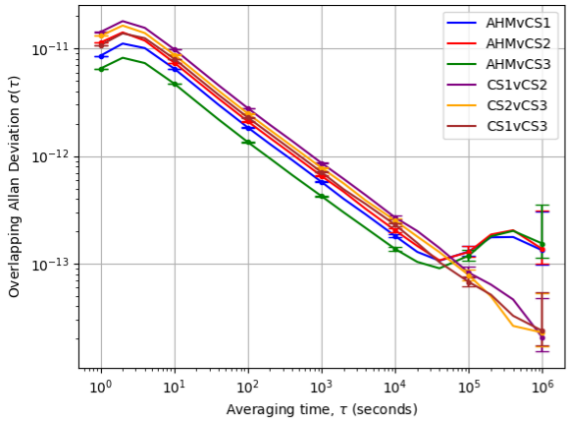

Fig. 1: Stability of individual clocks

performance comparison when all clocks were running for a continuous period of 31 days. From $\tau = 1$ second to $\tau = 10^4$ seconds, noise from cesium standards dominate. Maser noise becomes dominant after $\tau = 10^5$ seconds. Using the three-cornered hat method, one can infer from the plots that Cesium-3 is the most stable among all three cesium standards. The six phase measurements are converted to frequency before feeding it to the Kalman filter algorithms. The state space model of the filter consists of frequency and frequency drift values. Three different Kalman filters have been tested and the results are covered in the following sections. After obtaining the estimate updates from the Kalman filter, each clock is assigned specific weights and the weighted average of each frequency measurement is considered to be a paper clock.

An auxiliary output generator (AOG) is used to realize a physical signal corresponding to the paper clock. It takes the Cesium-3 (best among the three cesium standards) as a reference clock. Frequency offsets are calculated by comparing the AOG output obtained through the measurement system to the paper clock. These are fed to the AOG through an RS232 interface, *every second in real-time*. This provides a feedback loop type mechanism, which can be corrected at every time-step. We note that one need not do the feedback corrections to the AOG every second, rather, depending on the behavior of the clock the correction frequency can be determined.

At this stage, a free-running timescale is ready to be synchronized using GNSS signals. The AOG also has the property of syncing the output signal to a 1 PPS reference. It should be noted that the timescale is not being driven by

the GNSS signals, it is merely a sync using the NTP time transfer protocol [4].

B. Different Kalman Filter Methods

Over so many years, use of Kalman filters for timescales has increased manifold [5]. This paper includes the analysis of three tested filters, referred to as Linear Kalman filter (LKF) [6], Robust Kalman filter (RKF) [7], Outlier robust Kalman filter (ORKF) [8] on 30-day long continuous operation. LKF assumes a Gaussian noise distribution for all the measurements. The Kalman gain matrix $\boldsymbol{K}$ only depends on the covariance matrix. The RKF and ORKF are both based on the LKF and are designed to be robust to outliers and anomalous readings in different ways. Although their purposes are similar, their methods of handling these outliers differ greatly. These differences are contained within the update step of the Kalman Filter, as this is the step when a measurement is received. The prediction steps are the same as that of LKF.

Unlike the LKF, the RKF does not assume a Gaussian distribution of the noise but checks for a Gaussian distribution by performing a z-test on the residuals. A threshold is established above which a measurement is considered to be an outlier or a phase jump. It alters the measurement noise matrix ($\boldsymbol{R}$) and the state covariance matrix ($\boldsymbol{\Sigma}_x$). We define an adaptive factor (α) which modifies the predicted state covariance matrix ($\boldsymbol{\Sigma}_{\overline{x}}$) within the calculation of the Kalman gain ($\overline{\boldsymbol{K}}$) as seen in (1).

$$\overline{\boldsymbol{K}}_k = \frac{1}{\alpha_k} \cdot \boldsymbol{\Sigma}_{\overline{x}_k} \cdot \boldsymbol{H}^T \cdot \left(\frac{1}{\alpha_k} \cdot \boldsymbol{H} \cdot \boldsymbol{\Sigma}_{\overline{x}_k} \cdot \boldsymbol{H}^T + \overline{\boldsymbol{\Sigma}}_k \right)^{-1} \quad (1)$$

This reduces the influence of phase jumps on the state (x). Inflation factors (λ) are defined to construct an equivalent covariance matrix from $\boldsymbol{R}$ to reduce the influence of measurement outliers on predictions. Hence, by inflating the covariances, RKF manages to deal with phase jumps and measurement outliers in case of non-Gaussian distribution of residuals.

To calculate inflation factors, test statistics ($\overline{v}$) are first derived from the residuals between the predicted state ($\overline{x}$) and the measurement (z) using (2).

$$\overline{v}_i = \frac{\boldsymbol{H}\overline{x}_k - (z_k)_i}{\sqrt{tr(\boldsymbol{\Sigma}_{\overline{v}_k})}} \quad (2)$$

where k denotes the timestamps for dynamic elements and $\boldsymbol{\Sigma}_{\overline{v}}$ is the prediction residual vector covariance matrix given by (3).

$$\boldsymbol{\Sigma}_{\overline{v}_k} = \boldsymbol{H} \cdot \boldsymbol{\Sigma}_{\overline{x}_k} \cdot \boldsymbol{H}^T + \boldsymbol{R} \quad (3)$$

Then, the test statistics ($\overline{v}$) are compared to a tunable parameter (c). This parameter is the threshold defining outliers in terms of standard deviations. The inflation factors (λ) are calculated as follows

$$\lambda_{ii} = \begin{cases} 1 & |\overline{v}_i| \leq c \\ \frac{|\overline{v}_i|}{c} & |\overline{v}_i| > c \end{cases}, \quad (4)$$

and, $\lambda_{ij} = \sqrt{\lambda_{ii}\lambda_{jj}}$. Each element of $\boldsymbol{R}$ is then multiplied by the corresponding inflation factor to obtain the equivalent covariance matrix ($\overline{\boldsymbol{\Sigma}}$). This inflation of specific elements of $\boldsymbol{R}$ allows the filter to trust those elements of the measurement less, and thus the state is less affected.

On the other hand, the adaptive factor is used to inflate the elements of $\boldsymbol{\Sigma}_x$ related to the frequency states. This process seeks to correct $\boldsymbol{\Sigma}_{\overline{v}}$ to the theoretical noise covariance $\hat{\boldsymbol{\Sigma}}_{\overline{v}}$. The theoretical noise covariance can be found by taking the outer product of $\overline{v}$ and its transpose. α_k is then calculated as

$$\alpha_k = \begin{cases} 1 & otherwise \\ \frac{tr(\boldsymbol{\Sigma}_{\overline{v}_k} - \boldsymbol{R})}{tr(\hat{\boldsymbol{\Sigma}}_{\overline{v}_k} - \boldsymbol{R})} & tr(\hat{\boldsymbol{\Sigma}}_{\overline{v}_k}) > tr(\boldsymbol{\Sigma}_{\overline{v}_k}) \end{cases}, \quad (5)$$

On the other hand, the ORKF [8] treats observation noise as a hidden variable with student t-distribution. It also works with all additive noise types as it accounts for multiple, independent noise characteristics. Instead of $\boldsymbol{R}$, the ORKF uses $\boldsymbol{\Gamma}$ which is calculated as a convex combination of $\boldsymbol{R}$ and the expected outer product matrix with respect to a Gaussian distribution as shown in (6).

$$\boldsymbol{\Gamma}_k = \frac{s\boldsymbol{R} + \langle \delta\delta^T \rangle}{s+1} \quad (6)$$

Here s is equal to one less than the degrees of freedom. The outer product matrix is defined using the residuals (δ) between x and z:

$$\langle \delta\delta^T \rangle = (z_k - \boldsymbol{H}x_k)(z_k - \boldsymbol{H}x_k)^T + \boldsymbol{H}^T\boldsymbol{\Sigma}_{x_k}\boldsymbol{H} \quad (7)$$

where $\langle \cdot \rangle$ denotes expectation with respect to $\hat{\alpha}$ which follows a Gaussian distribution. This calculation inflates specific elements of $\boldsymbol{\Gamma}$ corresponding to elements of the measurement that are likely to be outliers. This ensures flexibility and the ability to deal with multiple noise characteristics simultaneously. Furthermore, while the degrees of freedom approach infinity, $\boldsymbol{\Gamma}$ converges to $\boldsymbol{R}$, i.e. with infinitely precise distribution of noise, the ORKF becomes a typical LKF.

Another significant aspect of the ORKF is in the iterative update step. The values of $\boldsymbol{K}$, x, $\boldsymbol{\Sigma}_x$, and $\boldsymbol{\Gamma}$, are repeatedly calculated until the values of x and $\boldsymbol{\Sigma}_x$ converge. During the first iteration of the update step, $\boldsymbol{\Gamma}$ is equal to $\boldsymbol{R}$, but each iteration following computes $\boldsymbol{\Gamma}$ and uses the new matrix in the next calculations of $\boldsymbol{K}$, x, and $\boldsymbol{\Sigma}_x$. The iterative nature of this step ensures that $\boldsymbol{\Gamma}$ reflects the significance of outliers in the measurement and x and $\boldsymbol{\Sigma}_x$ do not converge until the weights of the outliers are sufficiently diluted.

C. Different Mean Algorithms

Different weighting algorithms can have significant affect on the overall stability of the timescale as shown in fig. 3. Therefore, it is necessary to compare different filters with optimum weighting algorithms.

There are four weighting algorithms used to analyze the three Kalman filters. As a control to compare against the other algorithms, a static average is included in the fig. 2 which assigns equal weight to each frequency state, calculating an unbiased average. The other weighting algorithms are $K1$ [6], $K2$, and the Modified UTC Mean ($modUTC$) [7]. The comparison between the three weighting algorithms with all three filters can be seen in fig. (2).

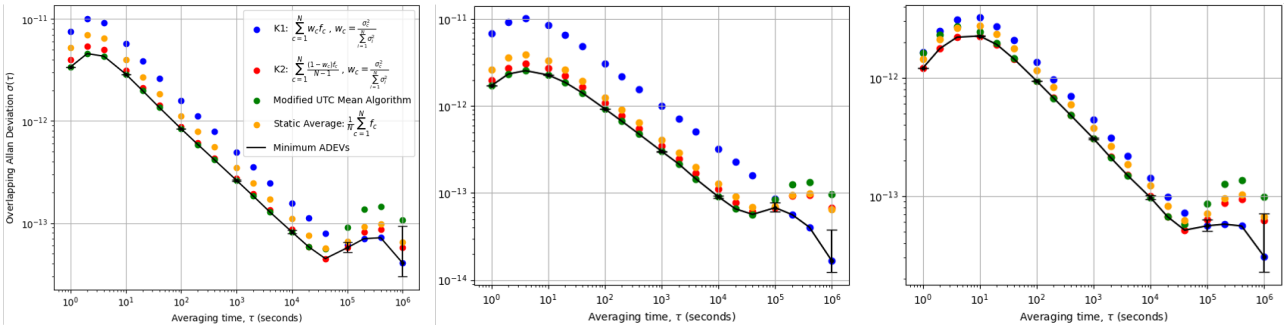

(a) Linear Kalman filter (LKF) (b) Robust Kalman filter (RKF) (c) Outlier robust Kalman filter (ORKF)

Fig. 2: Stability comparison of all 3 filters with all weighting algorithms

$K1$ and $K2$ use the same method to calculate weights, but differ in how those weights are used for weighted average. The weights are calculated using the frequency variances in the Kalman filter state covariance matrix as in (8).

$$w_i = \frac{\sigma_i^2}{\sum_{c=1}^{N} \sigma_c^2} \tag{8}$$

These weights are proportional to the variance of each frequency. $K1$ is calculated using (9),

$$K1 = \sum_{c=1}^{N} w_c f_c \tag{9}$$

In contrast, $K2$ gives more significance to the frequencies with lower variance. It uses (10),

$$K2 = \sum_{c=1}^{N} \frac{(1 - w_c) f_c}{N - 1} \tag{10}$$

The modified UTC mean algorithm differs from the previous algorithms in the fact that it recalculates the weights of each frequency every day, rather than at every time-step (one second). This algorithm seeks to reward predictable frequencies, and thus calculates weights based on the residuals (v) between the predicted states and the measurements received in a day-long interval using (11).

$$\sigma_i^2 = \frac{\sum_{j=1}^{D} \left(\frac{D+1-j}{D}\right) \epsilon_{i,j}^2}{\sum_{j=1}^{D} \left(\frac{D+1-j}{D}\right)} \tag{11}$$

where D is the number of measurements taken in the interval, i is the frequency corresponding to the variance being calculated, and $\epsilon_{i,j}$ is the jth prediction residual for the ith frequency. Moreover, the more recent measurements receive greater importance, as this data is more indicative of the predictability of the clock for the following interval. These variances are then used to derive the weights for each frequency using (12).

$$w_i = \frac{\frac{1}{\sigma_i^2}}{\sum_{c=1}^{N} \frac{1}{\sigma_c^2}} \tag{12}$$

All the measurements are averaged similar to $K1$, given as

$$modUTC = \sum_{c=1}^{N} w_c f_c \tag{13}$$

III. Results

Comparing the weighting algorithms, $K1$, $K2$, and $modUTC$, in fig. 2, we conclude that $modUTC$ is the best from $\tau = 1$ second till $\tau = 10^4$ seconds for both LKF and RKF. The ORKF algorithm, however shows an anomaly with $K2$, which performs better than $modUTC$ and gives the best short-term stability i.e. till $\tau = 10$ seconds.

The covariance matrix is computed at every time-step (one second in this case). Therefore, the AHM always has a lower covariance as compared to the cesium clocks. This becomes evident from the $K1$ weighting algorithm fig. 2 which follows the behavior of cesium clocks (higher covariance). This accounts for the lowest stability of $K1$ after $\tau = 10^5$ seconds. This behavior of $K1$ weighting algorithm is consistent for all three Kalman filters. On the contrary, the $K2$ tends to follow the trend of the AHM (lower covariance). A proof of concept is evident in the behavior of the stability curves (fig. 2), showing the static average is always between the $K1$ and $K2$.

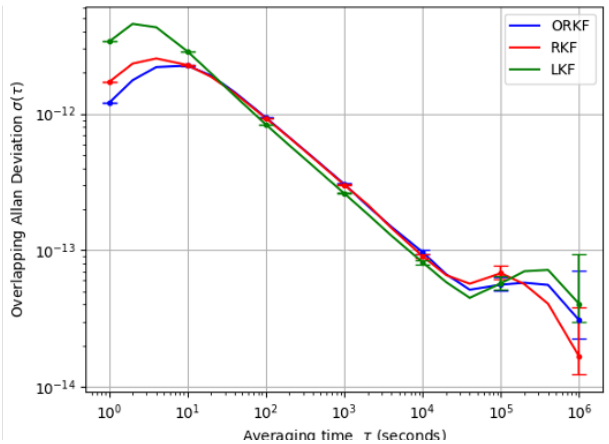

Fig. 3: Filter comparison

The fig. 3 shows the comparison between the best weighting algorithm for each of the three filters. It shows that ORKF performs the best until $\tau = 10$ seconds and RKF gives the best long-term stability ($\tau = 10^5$ seconds and beyond). Hence, a combination of ORKF for short term and RKF for medium to long-term stability output of a timescale would be a better choice.

IV. Conclusion and future work

The $K1$ weighting algorithm (based on higher covariances) proves to be the best choice at higher averaging times. The ORKF has been implemented and tested in timescale for the first time, and compared with the LKF and RKF.

The LKF is a better algorithm at shorter timescales, however the most interesting and useful algorithm is RKF, as it provides better estimation in medium to longer averaging times, and ORKF shows a consistent behaviour for K1 and K2 algorithms and would be a reasonable choice depending on the variability of the clocks used in a timescale. This work is intended as a basis for the future development and testing of machine-learning based neural network algorithms [1], [9]. Two more AHMs will be added to the timescale which will enhance the stability, performance and robustness. This timescale development will also allow us to build and test different time and frequency transfer techniques [10] with various other laboratories/metrology labs. Furthermore, this timescale may serve as a test-bed for characterizing the future SI definition algorithms [9], and testing of optical clocks within timescales, prior to their actual implementation for the UTC timekeeping.

Acknowledgments

We especially thank Dr. Adam Hauser (UA) for establishing the educational partnership with USNO. The cesium clocks for this work were provided by USNO. AHM support was provided by Mr. Bryan Owings, Microchip, Tuscaloosa, AL.

References

[1] T. Tanabe, J. Ye, T. Suzuyama, T. Kobayashi, Y. Yamaguchi, and M. Yasuda, "Potential for improving the local realization of coordinated universal time with a convolutional neural network," *Review of Scientific Instruments*, vol. 90, no. 12, p. 125 111, Dec. 2019, ISSN: 0034-6748. DOI: 10.1063/1.5088533. eprint: https://pubs.aip.org/aip/rsi/article-pdf/doi/10.1063/1.5088533/10033038/125111_1_online.pdf. [Online]. Available: https://doi.org/10.1063/1.5088533.

[2] N. Zimmerman, J. Pratt, M. Moldover, D. Newell, and G. Strouse, "The redefinition of the si: Impact on calibration services at nist," en, no. 10, 2015-06-01 2015. [Online]. Available: https://tsapps.nist.gov/publication/get_pdf.cfm?pub_id=918238.

[3] J. Quinn, "The BIPM and the accurate measurement of time," *Proc. IEEE*, vol. 79, no. 7, pp. 894–905, 1991. DOI: 10.1109/5.84965.

[4] "Ieee standard for a precision clock synchronization protocol for networked measurement and control systems," *IEEE Std 1588-2008 (Revision of IEEE Std 1588-2002)*, pp. 1–269, 2008. DOI: 10.1109/IEEESTD.2008.4579760.

[5] R. H. Jones and P. V. Tryon, "Estimating time from atomic clocks," *Journal of Research of the National Bureau of Standards*, vol. 88, no. 1, pp. 17–24, 1983. DOI: 10.6028/jres.088.002.

[6] L. A. Breakiron, "A kalman filter for atomic clocks and timescales," in *Proceedings of the 33rd Annual Precise Time and Time Interval Systems and Applications Meeting*, Long Beach, California, Nov. 2001, pp. 431–444.

[7] H. Song, S. Dong, L. Qu, X. Wang, and D. Guo, "A robust kalman filter time scale algorithm with data anomaly," *Journal of Instrumentation*, vol. 16, no. 06, P06032, Jun. 2021. DOI: 10.1088/1748-0221/16/06/P06032. [Online]. Available: https://dx.doi.org/10.1088/1748-0221/16/06/P06032.

[8] G. Agamennoni, J. I. Nieto, and E. M. Nebot, "An outlier-robust kalman filter," in *2011 IEEE International Conference on Robotics and Automation*, 2011, pp. 1551–1558. DOI: 10.1109/ICRA.2011.5979605.

[9] N. Dimarcq, M. Gertsvolf, G. Mileti, *et al.*, "Roadmap towards the redefinition of the second," *Metrologia*, vol. 61, no. 1, p. 012 001, Jan. 2024, ISSN: 1681-7575. DOI: 10.1088/1681-7575/ad17d2. [Online]. Available: http://dx.doi.org/10.1088/1681-7575/ad17d2.

[10] F. Arias, Z. Jiang, W. W. Lewandowski, and G. Petit, "Bipm comparison of time transfer techniques," in *Proceedings of the 37th Annual Precise Time and Time Interval Systems and Applications Meeting*, Vancouver, Canada, Aug. 2005, pp. 312–315.